International Journal of Automotive Technology, Vol. 20, No. 1, pp. 207–213 (2019)
DOI 10.1007/s12239–019–0020–0

pISSN 1229–9138/ eISSN 1976–3832

SIMULATION OF LIQUID AND GAS PHASE CHARACTERISTICS OF AERATED-LIQUID JETS IN QUIESCENT AND CROSS FLOW CONDITIONS

Kyoung-Su Im[1)], Zeng-Chan Zhang[1)], Grant Cook Jr.[1)], Ming-Chia Lai[2)] and Mun Soo Chon[3)*]

[1)]Livermore Software Technology Corporation, 7374 Las Positas Rd., Livermore, CA 94551, USA
[2)]Department of Mechanical Engineering, Wayne State University, MI 48202, USA
[3)]Department of Automotive Engineering, Korea National University of Transportation, Chungbuk 27469, Korea

(Received 30 November 2017; Revised 8 June 2018; Accepted 25 August 2018)

ABSTRACT–The simulation of the liquid- and gas-phase properties of aerated-liquid jets in various quiescent and cross flow conditions are presented in the study. For simplicity, water is used as the liquid for all test conditions. The effect of various air-to-liquid ratios under super-sonic cross flow conditions are simulated and compared to experimental conditions, which is taken in the supersonic wind tunnel with a dimension of 762 × 152 × 127 mm. An injector with an orifice diameter of 0.5 mm is used both in a non-aerated and aerated injection into a supersonic cross flow prescribed by the momentum flux ratio of the liquid jet to free stream air, q_0. The initial conditions of the spray calculation were estimated from internal flow simulation using VOF and X-ray data. The conservation-element and solution-element (CE/SE) method, a novel numerical framework for general conservation law, is applied to simulate the compressible flow. The effect of degree of aeration, breakup, and mixing of the liquid spray are demonstrated. The spray penetration height and average droplet size along with a spray penetration axis are quantitatively compared with data. The shock train flow structures induced by the presence of a liquid jet are further discussed.

KEY WORDS : Liquid jet, Cross flow, Aerated injection, Spray penetration, Breakup, CE/SE method

NOMENCLATURE

c_p, c_v : specific heat constants
C_D : drag coefficient
D : drag function or drop diameter
d_0 : nozzle diameter
e : specific internal energy
E : specific total energy
h_0 : penetration height
$L(T)$: heat of vaporization
$M_{x,y,z}$: momentum exchange terms
M_s : free stream Mach number
M_0 : initial mass
m : mass
p : pressure
q_x, q_y, q_z : heat flux
Q_s : energy exchange term
r : jet radius or drop radius
Re : Reynolds number
u, v, w : velocities
t : time
γ : ratio of specific heats
μ : viscosity
ρ : density
σ : surface tension coefficient
τ : viscous stress

SUBSCRIPTS

g : gas
k : particle index
l : liquid
x, y, z : spatial coordinates
0 : initial value

*Corresponding author. e-mail: mschon@ut.ac.kr

1. INTRODUCTION

The design of the modern propulsion system including a liquid-fueled and air-breathing aircraft engine depends on liquid atomization performance, which can be determined by the spray mixing and penetration into high speed free stream air and it eventually determines the combustion efficiency of the combustor. One efficient method to accomplish better atomization is the aeration technique, which involves an injection process both a gas phase and liquid phase together in a single injector. As a result, the breakup and momentum penetration are maximized (Lin *et al*., 2001, 2002a, 2002b, 2004). The breakup process

including deformation, liquid fragmentation, and completing disintegration is mostly dictated by two independent non-dimensional numbers, the Weber number and Ohnesorge number in conjunction with the characteristic breakup time (Hsiang and Faeth, 1992; Ranger and Nicholls, 1969).

Hsiang and Faeth (1992) presented the deformation and breakup regime map for the drop breakup, showing transitions as functions of Weber and Ohnesorge numbers. They categorized the breakup regime into different transitions considering more detailed deformations, i.e., non-oscillatory and oscillatory deformations, bag breakup, multimode breakup, shear breakup, and catastrophic breakup. Wu *et al*. (1997) characterized the near-field jet breakup process as three different regimes: liquid column, ligament, and droplet regimes.

Ranger and Nicholls (1969) have been the first to use the characteristic breakup time to demonstrate the effects of the high free-stream velocity (M_s = 1.5 ~ 3.5) on drop deformation, displacement, and breakup time, i.e., the time for the complete breakup process. By sending a shock wave across water droplets with diameters in the range of 750 ~ 4400 μm, they provided the parametric data on droplet disintegration rate, droplet displacement, and droplet breakup time using dimensionless form near the catastrophic breakup regime. They also provided a theoretical relation for the rate of mass reduction, the mass stripped away from the drop surface by utilizing the equations from Taylor's analysis (Taylor, 1963).

Lin *et al*. have applied the phase Doppler particle analyzer (PDPA), which has been utilized extensively in the spray research, to view the atomization performance by measuring the spray droplets, penetration, and spray plume using an aerated injector (Lin *et al*., 2001, 2002a, 2002b, 2004).

However, so far only limited numerical results have been reported regarding the spray properties with the high-speed cross flow due to the difficulty in the complex breakup processes in aerated injection. Therefore, as an extension of the previous our research (Im *et al*., 2011), the objective of the present study is to continue the investigation on the penetration heights, and spray structures of non-aerated and aerated liquid jets in a supersonic cross flow environment. Furthermore, the flow structures induced by the liquid jets are investigated.

2. NUMERICAL METHOD

2.1. Gas Phase Models

The governing systems of the supersonic gas phase flow with interacting spray particles are the 3-D unsteady compressible Navier-Stokes equations and can be given in the vector form as,

$$\frac{\partial}{\partial t}\begin{Bmatrix}\rho\\ \rho u\\ \rho v\\ \rho w\\ \rho E_t\end{Bmatrix}+\frac{\partial}{\partial x}\begin{Bmatrix}\rho u\\ \rho u^2+P-\tau_{xx}\\ \rho uv-\tau_{xy}\\ \rho uw-\tau_{xz}\\ (\rho E_t+P)u-\beta_x\end{Bmatrix}+\frac{\partial}{\partial y}\begin{Bmatrix}\rho v\\ \rho uv-\tau_{xy}\\ \rho v^2+P-\tau_{yy}\\ \rho vw-\tau_{yz}\\ (\rho E_t+P)v-\beta_y\end{Bmatrix}+\frac{\partial}{\partial z}\begin{Bmatrix}\rho w\\ \rho uw-\tau_{xz}\\ \rho vw-\tau_{yz}\\ \rho w^2+P--\tau_{zz}\\ (\rho E_t+P)w-\beta_z\end{Bmatrix}=\begin{Bmatrix}0\\ M_x\\ M_y\\ M_z\\ Q_s\end{Bmatrix} \tag{1}$$

where t, x, y, and z, are the time, x-, y- and z-direction coordinates, respectively. The variables of r, u, v, w, p, and E_t defined in the flow and the flux vectors represent density, x-, y-, and z-velocity, pressure, and specific total energy of the gas phase, respectively. The specific total energy E_t is defined as

$$E_t = e+\frac{1}{2}(u^2+v^2+w^2) \tag{2}$$

where $e = p/(\gamma-1)$ is the internal energy of the gas phase, and $\gamma = c_p/c_v$ is the ratio of specific heats. The components of the viscous stress, τ_{xx}, τ_{yy}, τ_{zz}, τ_{xy}, τ_{yz}, and τ_{xz} are given in (Tannehill *et al*., 1997) and the viscous vector in the energy equation is given by

$$\begin{aligned}\beta_x &= u\tau_{xx}+v\tau_{xy}+w\tau_{xz}-q_x\\ \beta_y &= u\tau_{xy}+v\tau_{yy}+w\tau_{yz}-q_y\\ \beta_z &= u\tau_{xz}+v\tau_{yz}+w\tau_{zz}-q_z\end{aligned} \tag{3}$$

Here, q_x, q_y, and q_z are the terms describing the heat transfer by conduction and given by Fourier's law (Tannehill *et al*., 1997). The source terms appear on the right-hand side of the Equation (1) account for effects due to the particle interaction. In present study, we assumed the non-evaporating spray, so that there is no source term in the continuity equation. The M_x, M_y, and M_z in the momentum equations are the terms defining the x, y, and z momentum exchanges induced by spray particles in the differential control volume. The term, Q_s in the energy equation represents the work done by the particles on the gas.

$$\mathbf{M}_i = -\frac{d}{dt}(m\mathbf{u})_k,\ i = x, y, z \tag{4}$$

$$Q_s = -\frac{d}{dt}(mE_t)_k \tag{5}$$

The space-time conservation element solution element (CESE) method has been applied to solve the shock-spray interacting flow (Zhang *et al*., 2002). The space-time CESE method is a high-resolution and genuinely multidimensional method for solving conservation laws. It has a solid foundation in physics and yet is simple in mathematics. Its nontraditional features are: (i) a unified treatment of space and time, (ii) the introduction of

conservation element (CE) and solution element (SE) as the vehicles for enforcing space-time flux conservation, and (iii) a time marching strategy that has a space-time staggered stencil at its core and, as such, can capture shocks without using Riemann solvers. Note that conservation elements are non-overlapping space-time subdomains introduced such that (i) the computational domains can be filled by these subdomains; and (ii) flux conservation can be enforced over each of them and also over the union of any combination of them. On the other hand, solution elements are non-overlapping space-time subdomains introduced such that (i) the boundary of any CE is covered by a combination of SEs; and (ii) within a SE, any physical flux vector is approximated using a simple smooth function.

2.2. Spray Models

For a spray flow in a Lagrangian reference frame, a computational particle represents a finite number of particles having the same diameter, velocity, and temperature (Dukowicz, 1980). Then, the particle position is given by

$$\frac{d\mathbf{x}_k}{dt} = \mathbf{u}_k \tag{6}$$

The rate of particle momentum change is given by enforcing the conservation law of an individual particle and can be expressed as,

$$m_k \frac{d\mathbf{u}_{k,i}}{dt} = F_i \tag{7}$$

where $m_k = 4\pi\rho r^3/3$ is the mass of the spray droplet. F_i is the force acting on the droplet due to aerodynamics drag and gravitational force. The drag coefficient, typically determined by a empirical relation and is given for the supersonic flow as (Crowe *et al*., 1998),

$$C_D = 2 + (C_{D,0}-2)_{exp}\left(-3.07\sqrt{\gamma}g(\mathrm{Re}_k)\frac{M}{\mathrm{Re}_k}\right) + \frac{h(M)}{\sqrt{\gamma}M}\exp(-\mathrm{Re}_k/2\,\mathrm{M}) \tag{8}$$

where g(Re) and h(M) are given by,

$$g(\mathrm{Re}_k) = \frac{1+\mathrm{Re}_k(12.278+0.548\mathrm{Re}_k)}{1+11.278\mathrm{Re}_k} \tag{9}$$

$$h(M) = \frac{5.6}{1+M} + 1.7\sqrt{\frac{T_k}{T_g}} \tag{10}$$

In Equation (8), $C_{D,0}$ is the standard drag coefficient and is given by,

$$C_{D,0} = \frac{24}{\mathrm{Re}_k}\left[1.0+0.15\mathrm{Re}_k^{0.687}\right] \quad \mathrm{Re}_k < 10^3$$
$$= 0.44 \quad \mathrm{Re}_k > 10^3 \tag{11}$$

where Re_k is the particle Reynolds number evaluated by a relative velocity between the surrounding gas and particle, i.e.,

$$\mathrm{Re}_k = \frac{2r_k|u_i - u_{k,i}|\rho_g}{\mu} \tag{12}$$

The energy equation of the droplet is also given by

$$m_k \frac{de_k}{dt} = L(T_k)\frac{dm_k}{dt} + 4\pi r_k^2 \dot{q}_k \tag{13}$$

where $L(T_k)$ is the heat of vaporization and $\dot{q}_k$ is the rate of heat conduction to the particle surface per unit area. In the present study, Equations (6) ~ (13) are the system equations for simulating the spray flow in conjunction with the supersonic cross flow. The initial conditions of the spray calculation were estimated from internal flow simulation using VOF and X-ray data.

3. RESULTS AND DISCUSSIONS

In the present study, all thermodynamic variables, test conditions and geometrical parameters in numerical calculation were brought from reference (Lin *et al*., 2004). Water was used as the test liquid in the present calculation, which has a density of 998 kg/m^3, water viscosity of 2.67 × 10^{-3} kg/m·s, and surface tension of 0.072 N/m. Initially, the total pressure and temperature inside of the test section were maintained at 206 kPa and 533 K, respectively. Then, the corresponding static pressure and temperature under the isentropic assumption are converted to give 29 kPa and 304.1 K with flow velocity of 678.13 m/s, which is based on the free-stream Mach number of 1.94. The jet-to-air momentum flux ratio, q_0, which is defined as a ratio of $\rho_L v_j^2/\rho_\infty v_\infty^2$, was used to calculate the injection velocity of the spray jet. The test section of the calculation domain has a height of 127 mm, width of 152 mm, and length of 762 mm. The injection nozzle diameter of 0.5 mm located at 139 mm from the leading edge of the test section was used as a spray injector. A pure liquid injection case (P0) and two cases (A1 and A2, see Table 1) for GLR defined as aerating gas to liquid mass ratio are selected for the comparisons and the validation with experimental data. In case P0, the liquid condition for the cross-section area of 0.5 mm nozzle diameter was used. However, the aerated spray conditions are not straightforward because two phase injections are required in nozzle exit. Thus, we simplified the situation based on following assumptions: 1) a steady-state flow, 2) two separated flow regimes with annular liquid outside and choked and under-expanded air inside

Table 1. Test conditions.

Case	T_0 (K)	D_0 (mm)	x/d_0	q_0	GLR (%)
P0	533	0.5	200	7	0
A1	533	0.5	200	7	2
A2	533	0.5	200	7	5

Table 2. Comparisons of the flux averaged droplet size and velocity.

SMD (μm)		u_p/u_∞ (%)	
Exp. data	Simulation	Exp. data	Simulation
15.2	17.1	70.8	70.5
13.8	12.8	83.3	75.5
13.2	12.5	86.5	76.5

the core which is a fraction of the exit cross-section area. For the results presented in the paper, a fixed 60 % cross-sectional area is assumed for the air core. The thermal dynamic properties and exit velocity of each phase can then be determined accordingly.

For validation purposes as a reference for the accuracy of the simulation, the flux-averaged SMD data for the non- and aerated liquid jets are compared to the experimental counterparts, which are calculated on the *y*-*z* plane at x = 100 mm between the t = 1.5 ms to 2.5 ms time instants. In aerated cases, the simulation results both in SMD and velocity ratio between the spray and free stream that agree with experimental data as can be seen in Tables 1 and 2.

Figure 1 (a) shows the simulation results for the axial view of overall cross-sectional spray structure compared to the shadow graphic flow visualization (see Figure 1 (b)) for the non-aerated case, P0. Also shown in Figure 1 (c) are comparisons of the spray penetration heights for the simulation and experimental data derived from the empirical correlations both in shadow graphic data and the PDPA measurement. In general, the spray structures agree well in both cases. The correlations in the shadow and PDPA measurement for the spray penetration heights are given respectively as,

$$Shadow: \quad \frac{h_0}{d_0} = 3.94 \cdot q_0^{0.47} (x/d_0)^{0.21} \tag{14a}$$

$$PDPA: \quad \frac{h_0}{d_0} = 4.73 \cdot q_0^{0.30} (x/d_0)^{0.30} \tag{14b}$$

Although they are using the same test facility and injectors, the derived correlations are different in Figure 1 (c), where the spray penetration heights measured by the shadowgraph are consistently lower than those measured using PDPA. The simulation results are slightly lower than those of using PDPA and higher than those of using shadowgraph, indicating that the results are moderately acceptable with different diagnostics.

Figure 2 shows the overall sprays for the non-aerated (GLR = 0 %), and aerated with GLR = 2 % and GLR = 5 % cases. As can be seen, the spray penetrations for the aerated cases are higher than those of the non-aerated case. The spray penetration height is a key factor in determining the performance of a fuel injector in high speed air breathing combustor since the incoming high-speed free stream air

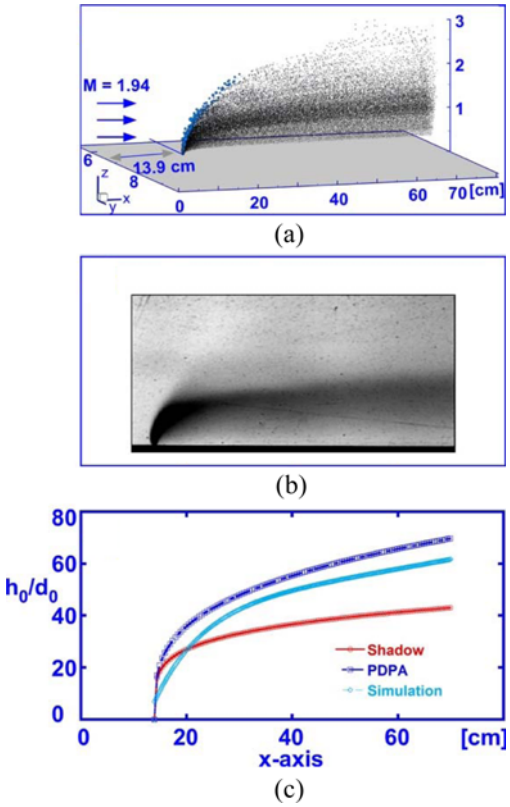

Figure 1. Cross flow structures compared with a shadowgraph image and penetration heights in the baseline case.

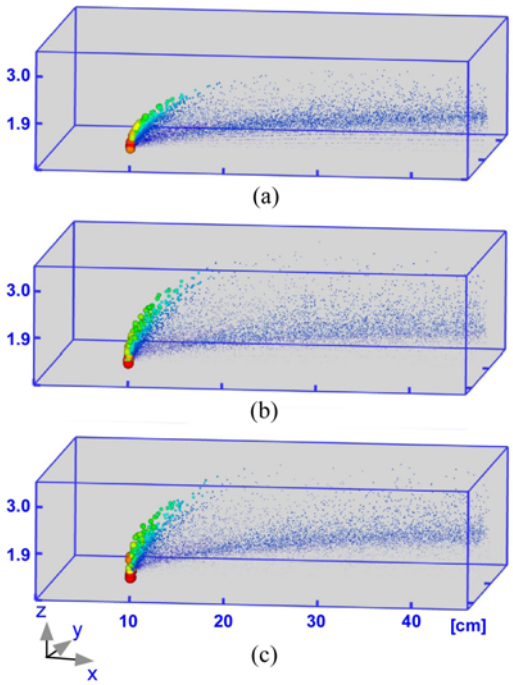

Figure 2. Cross flow structures compared with a shadowgraph image and penetration heights in the baseline case.

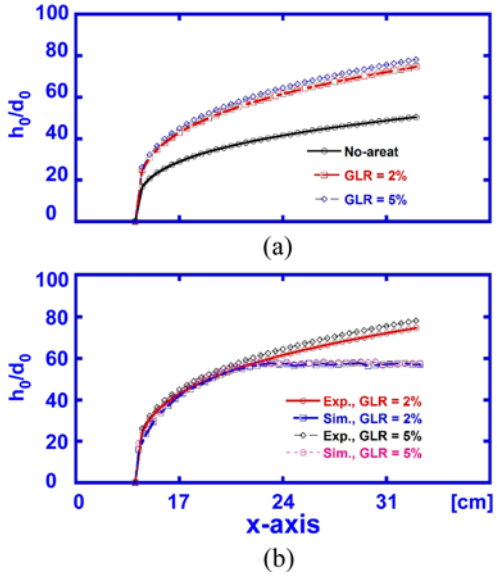

Figure 3. Penetration heights of the non-aerated and aerated liquid jets: (a) Drawing by empirical equations; (b) Results compared with experimental data.

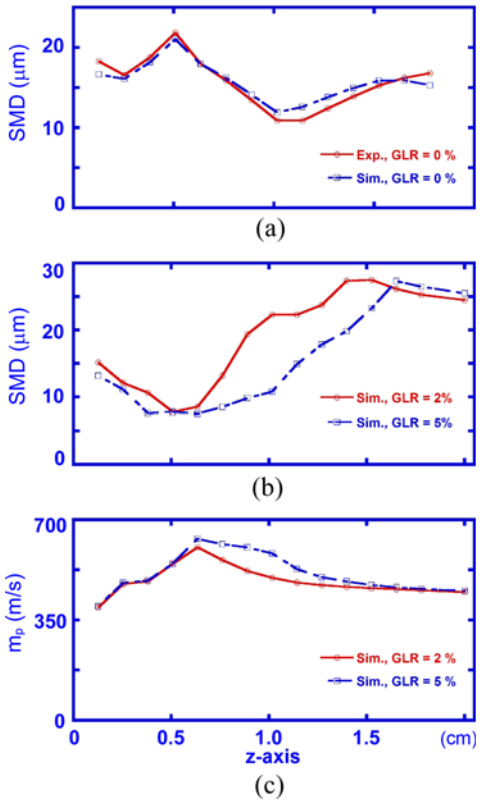

Figure 4. Droplet size and axial velocity: (a) Non-aerated and PDPA measurement at $x/d_0 = 100$; (b) Droplet sizes of GLR = 2 % conditions and GLR = 5 % at $x/d_0 = 200$; (c) Axial velocities of GLR = 2 % and GLR = 5 % conditions at $x/d_0 = 200$.

has a large momentum. The main purposes of the aerated liquid jets are shown to support the momentum transfer to the liquid spray for better penetration and improve the atomization of the liquid column prior to injection. Although it is not clearly distinguishable in the aerated cases as shown in Figures 2 (b) and (c), it is clear that the aerated sprays show higher penetration and much better atomization on the downstream of the spray injector.

Figure 3 (a) illustrates the spray penetration heights of the non-aerated and two aerated cases calculated from the experimental correlations by PDPA measurement. Figure 3 (b) shows the comparisons of those results between the experiments and the simulations. As shown in the figures, the spray penetration heights of the aerated cases are quite a bit higher than those of the non-aerated case for a short time after injection. However, the spray penetrations for the aerated cases are not distinguishable in both the experiment and the simulation. It is interesting to see that the curves of the experiment and the simulation start to separate at about $x = 20$ cm. The penetration curves from the correlation are continuously increasing along with the spray axis, but the simulation results are slightly changed and seem to converge to a certain value. Note that the prediction from the simulation is more reasonable since it may not possible for the spray droplets to continuously penetrate into a high speed free stream, which has a large amount of momentum.

More validation with data can be seen in Figure 4 (a) where the measured SMD distribution was compared with simulation results at $x/d_0 = 100$ along the y-direction, under the same operating condition of the pure liquid jets without aerated injection. The agreement between the measured data and simulation is quite good although there are non-coincident regions at the lowest and highest sections of the spray. With increased confidence, we further explored the droplet size and axial droplet velocity distribution along with the penetration axis for two aerated injection cases, GLR = 2 % and 5 % at axial position at $x/d_0 = 200$. The curve trends for both cases are similar such that the droplet size from the bottom shows slightly decreasing and it is apparently increased at the main stream of the spray in both cases. In addition, the droplet size distributions are a little smaller in case of GLR = 5 %, indicating that the more aeration promises better atomization and thus easily obtains the flow stream momentum resulting in the higher axial velocity.

Figure 5 shows the near views of the aerated sprays separated from the full calculating geometry. We note that it is extremely difficult, if not impossible, to clearly view the near nozzle regimes with an experiment method and also in simulation for the 3-dimentional geometry. To this end, we designed the simulation domain with three different parts using LS-DYNA pre-post software (LS-PrePost, 2017). Upon the completing the calculation, the results thus can be separately displayed for each part of the domain. In the present study, we divided two front parts by

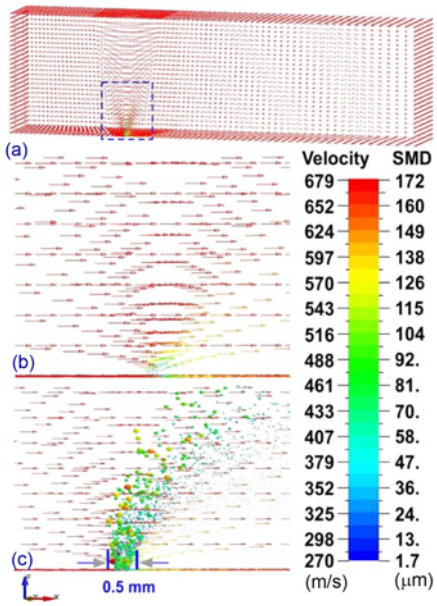

Figure 5. Closed nozzle views of the aerated spray both in air flow and droplets for the case A1.

the center line to $x/d_0 = 200$ (100 mm) from the nozzle and another part for the whole domain after the front two sections starting at $x/d_0 = 200$. Figure 5 (a) shows one of the front parts clearly showing the center plane of the domain. However, it is not clear enough to see the near nozzle with flow vectors and spray injections since the computational domain is still much bigger than the nozzle diameter (= 0.5 mm).

The dot lined rectangular inset in Figure 5 (a) was thus zoomed up in Figures 5 (b) and (c), respectively, for the investigation of the cross flow and spray phenomenon. The velocity vectors are mostly parallel to the flow direction as can be seen in Figure 5 (b). For the present study, 60 % of the inner cross-sectional area with 0.5 mm diameter is choked to given GLR conditions, meaning that the sonic speed with corresponding pressure and temperature are prescribed at inner area. Although the air injection velocities are 340 m/s, the cross velocities (~ 678 m/s) could be too high, so that the injected air may not seem to be penetrated sufficiently into the high speed free stream. However, it should be noted that the aerated spray droplets could penetrate higher than those of the non-aerated as can be seen in Figure 3 (a). The spray flow is directly overlapped into the gas flow field as shown in Figure 5 (c). Since the injected liquid drop first undergoes the surface primary breakup, as a result, the small droplets are stripped from the main stream of the liquid column. With aid of the aerated momentum, the injected droplets penetrate well into the free stream, where the big drops are in front of spray and the small drops are in the leeward side of the liquid surface. Close to the nozzle area, a highly dense spray like a liquid column is observed. To resolve the aerated injection, we constructed a total 5 mesh points in the nozzle diameter of 0.5 mm. Thus, the characteristic element size is about 100 micrometer.

As a result, the volume fraction of the gas to liquid mixture occupied by the liquid can exceed that of the gas in a certain control volume, which is called the "churning flow" regime (O'Rourke, 1981), since the injected particle SMD is about 100 microns. In such a regime, the liquid exists as sheets, filaments, or lattice in a physical situation, so that the only way to continue the simulation is by either using a one-way coupling technique or through the ghost fluid method (Fedkiw *et al*., 1999). In the present study, we used the conditional coupling technique limiting two way coupling into higher gas volume fraction cells such as those with characteristic length of 0.5 mm.

In our previous research (Im *et al*., 2011), we discussed that the 3-dimensional shock wave structures developed due to the liquid jets from the bottom nozzle when the normal shock wave propagates into flow direction, the conical shock wave first developed from the position where the liquid jet is injected. Although the developed 3-dimensional conical shock structures are not illustrated in this paper, the same phenomenological structures are constructed in the aerated injections. However, again, it is not so clear if the reflected shock waves affect the mixing process of the liquid jet and thus combustion processes.

4. CONCLUSION

A study of the numerical simulation for the spray analysis in the cross flow has been conducted with non- and aerated liquid jets injection without and with GLR conditions. To simulate a highly compressible flow in supersonic wind tunnel, we employed a novel numerical simulation technique based on the general conservation law, the conservation-element and solution-element (CE/SE) method. The spray penetration heights were validated with different diagnostics, shadowgraph and PDPA measurement. In addition, the drop size distribution was also validated with the experimental data. In both cases, we proved that our simulation results are in quite good agreement with the data. With confidence from this validation, we further explored and demonstrated the effect of the aeration on the spray penetrations and atomization and it was found that the aerated injections are necessitated for the spray droplets to penetrate into a large momentum free stream flow. We also demonstrated the shock wave structures in the flow channel, which are induced by the liquid jets from the bottom nozzle. However, it is not clear whether the shock wave structures improve the mixing process of the liquid jet and thus combustion processes, and thus remain future research topics.

REFERENCES

Crowe, C. T., Sommerfield, M. and Tsuii, Y. (1998).

Multiphase Flows with Droplets and Particles. CRC Press. Boca Raton, Florida, USA.

Dukowicz, J. K. (1980). A particle-fluid numerical model for liquid sprays. *J. Computational Physics* **35**, **2**, 229–253.

Fedkiw, R., Aslam, T., Merriman, B. and Osher, S. (1999). A non-oscillatory Eulerian approach to interfaces in multimaterial flows (the Ghost Fluid Method). *J. Computational Physics* **152**, **2**, 457–492.

Im, K..-S., Lin, K.-C., Lai, M.-C. and Chon, M. S. (2011). Breakup modeling of liquid jet in cross flow. *Int. J. Automotive Technology* **12**, **4**, 489–496.

Hsiang, L.-P. and Faeth, G. M. (1992). Near-limit drop deformation and secondary breakup. *Int. J. Multiphase Flow* **18**, **5**, 635–652.

Lin, K.-C., Kennedy, P. J. and Jackson, T. A. (2001). Spray structures of aerated-liquid jets in subsonic crossflows. *39th Aerospace Sciences Meeting and Exhibit*., Reno, Nevada, USA.

Lin, K.-C., Kennedy, P. J. and Jackson, T. A. (2002). Penetration heights of liquid jets in high-speed cross flows. *40th AIAA Aerospace Sciences Meeting and Exhibit*., Reno, Nevada, USA.

Lin, K.-C., Kennedy, P. J. and Jackson, T. A. (2002). Structures of aerated-liquid jets in high-speed cross flows. *32nd AIAA Fluid Dynamics Conf. and Exhibit*., St. Louis, Missouri, USA.

Lin, K.-C., Kennedy, P. J. and Jackson, T. A. (2004). Structures of water jets in a Mach 1.94 supersonic crossflow. *42nd AIAA Aerospace Sciences Meeting and Exhibit*., Reno, Nevada, USA.

LS-PrePost (2017). http://www.lstc.com/products/ls-prepost

O'Rourke, P. J. (1981). *Collective Drop Effects in Vaporizing Liquid Spray*. Ph. D. Dissertation. Princeton University. Princeton, New Jersey, USA.

Ranger, A. A. and Nicholls, J. A. (1969). Aerodynamic shattering of liquid drops. *AIAA Journal* **7**, **2**, 285–290.

Tannehill, J. C., Anderson, D. A. and Pletcher, R. H. (1997). *Computational Fluid Mechanics and Heat Transfer*. 2nd edn. CRC Press. Boca Raton, Florida, USA.

Taylor, G. I. (1963). *The Shape and Acceleration of a Drop in High Speed Air Stream*. The Scientific Papers of G. I. Taylor. Vol. 3.

Wu, P.-K., Kirkendall, K. A., Fuller, R. P. and Nejad, A. S. (1997). Breakup processes of liquid jets in subsonic crossflows. *J. Propulsion and Power* **13**, **1**, 64–73.

Zhang, Z.-C., Yu, S.-T. and Chang, S.-C. (2002). A space-time conservation element and solution element method for solving the two- and three-dimensional unsteady Euler equations using quadrilateral and hexahedral meshes. *J. Computational Physics* **175**, **1**, 168–199.